Elsevier Editorial System(tm) for Carbohydrate Polymers

Manuscript Draft

Manuscript Number: CARBPOL-D-17-04421R1

Title: Phase separation in amorphous hydrophobically-modified starch - sucrose blends: Glass transition, matrix dynamics and phase behavior

Article Type: Research Paper

Keywords: OSA starch; Sucrose; Glass transition; Amorphous phase separation; Solid-state NMR; Differential scanning calorimetry

Corresponding Author: Dr. Job Ubbink,

Corresponding Author's Institution: California Polytechnic State University

First Author: David Hughes

Order of Authors: David Hughes; Gabriela Badolato Bonisch; Thomas Zwick; Christian Schaefer; Concetta Tedeschi; Bruno Leuenberger; Francesca Martini; Giacomo Mencarini; Marco Geppi; M. Ashraf Alam; Job Ubbink

Abstract: The phase behavior and matrix dynamics of amorphous blends of octenyl succinic anhydride (OSA) modified starch and sucrose was studied as function of blend composition and water content. Phase separation into two amorphous phases, one enriched in OSA starch and the other in sucrose, was confirmed by differential scanning calorimetry (DSC). DSC and ^{1}H solid-state NMR show that the phase separation is only partial. The glass transition temperature (T_g) of the OSA starch-rich phase was found to be $\sim$ 30-100 K higher than the T_g of the sucrose- rich phase, depending on blend composition and water content. A novel type of coupling between changes in physical state of the sucrose-rich phase and plasticizer redistribution is proposed, leading to an unexpected increase of the glass transition temperature of the modified starch-rich phase at higher matrix water contents. A quantitative model for the phase separation of the anhydrous blends into two amorphous phases is presented. The model predicts that, with increasing blend sucrose content, the weight fraction of the sucrose-rich phase decreases, while the sucrose content of both the OSA starch-rich phase and the sucrose-rich phase increases. This novel phenomenon is relevant in the understanding of the stability and performance of multiphase food and pharmaceutical components.

Phase separation in amorphous hydrophobically-modified starch - sucrose blends: Glass transition, matrix dynamics and phase behavior.

David J. Hughes[a], Gabriela Badolato Bönisch[b], Thomas Zwick[b], Christian Schäfer[b], Concetta Tedeschi[b], Bruno Leuenberger[b], Francesca Martini[c], Giacomo Mencarini[c], Marco Geppi[c], M. Ashraf Alam[a], Job Ubbink[d,a,e,*]

[a] *H. H. Wills Physics Laboratory, University of Bristol, Tyndall Avenue, Bristol BS8 1TL, United Kingdom*
[b] *DSM Nutritional Products Ltd, Research Center Formulation & Application, P.O. Box 2676, 4002, Basel, Switzerland*
[c] *Dipartimento di Chimica e Chimica Industriale, Universitá di Pisa, via Moruzzi 13, 56124 Pisa, Italy*
[d] *Food Science and Nutrition Department, California Polytechnic State University, 1 Grand Ave., San Luis Obispo, CA 93407*
[e] *Food Concept & Physical Design "The Mill", Mühlweg 10, CH-4112 Flüh, Switzerland*

Abstract

The phase behavior and matrix dynamics of amorphous blends of octenyl succinic anhydride (OSA) modified starch and sucrose was studied as function of blend composition and water content. Phase separation into two amorphous phases, one enriched in OSA starch and the other in sucrose, was confirmed by differential scanning calorimetry (DSC). DSC and ^{1}H solid-state NMR show that the phase separation is only partial. The glass transition temperature (T_g) of the OSA starch-rich phase was found to be $\sim$ 30-100 K higher than the T_g of the sucrose-rich phase, depending on blend composition and water content. A novel type of coupling between changes in physical state of the sucrose-rich phase and plasticizer redistribution is proposed, leading to an unexpected increase of

*Corresponding author at: Food Concept & Physical Design "The Mill". Tel.: +41 61 271 12 51

Email addresses: d.j.hughes@bristol.ac.uk (David J. Hughes), gabriela.badolato@dsm.com (Gabriela Badolato Bönisch), thomas.zwick@dsm.com (Thomas Zwick), christian.schaefer@dsm.com (Christian Schäfer), cc.tedeschi@gmail.com (Concetta Tedeschi), bruno.leuenberger@bluewin.ch (Bruno Leuenberger), francesca.martini@pi.iccom.cnr.it (Francesca Martini), giacomomencarini1@gmail.com (Giacomo Mencarini), marco.geppi@unipi.it (Marco Geppi), m.a.alam@bristol.ac.uk (M. Ashraf Alam), jubbink@calpoly.edu (Job Ubbink)

the glass transition temperature of the modified starch-rich phase at higher matrix water contents. A quantitative model for the phase separation of the anhydrous blends into two amorphous phases is presented. The model predicts that, with increasing blend sucrose content, the weight fraction of the sucrose-rich phase decreases, while the sucrose content of both the OSA starch-rich phase and the sucrose-rich phase increases. This novel phenomenon is relevant in the understanding of the stability and performance of multiphase food and pharmaceutical components.

Keywords: OSA starch, Sucrose, Glass transition, Amorphous phase separation, Solid-state NMR, Differential scanning calorimetry

---

1. Introduction

One of the principal applications of microencapsulation is to protect sensitive actives during storage against the detrimental effects of water and atmospheric oxygen. In most cases such protective matrices consist of amorphous carbohydrates in the glassy state, so-called glass encapsulation systems (Ubbink, 2016). Non-optimal barrier properties of the encapsulation matrix lead to increased rates of chemical degradation, mainly by oxidation, of the encapsulated actives (Karel, 1990). In addition, the active may prematurely diffuse out of the matrix into the environment. It is therefore of significant importance to optimize the formulation of carbohydrate-based encapsulation matrices in order to maximize the barrier properties and thereby improve the stability and shelf life of microencapsulated actives (Ubbink et al., 2008; Reineccius & Yan, 2016).

At the molecular level, barrier properties are governed by two parameters: the solubility and the mobility (diffusivity) of the permeating compounds in the barrier material. The mobility of small molecules, such as water and oxygen, in glassy carbohydrates was initially believed to be governed primarily by the proximity of the glass transition temperature (T_g) of the matrix to the temperature of the storage environment (Levine, 2002). It has since been recognized that this interpretation of molecular mobility is inadequate (Ubbink & Krüger,

2006; Cicerone & Douglas, 2012; Cicerone et al., 2015; Ubbink, 2016). While the mobility of the larger carbohydrate molecules that constitute the matrix is governed by the α-relaxation and therefore effectively cease at temperatures below T_g, the mobility of smaller molecules in the matrix is thought to be related to the β-relaxation and remains appreciable even in the glassy state (Cicerone & Douglas, 2012). The β-relaxation, which is in turn hypothesized to be related to the molecular packing of the matrix in the glassy state, can be directly probed by positron annihilation lifetime spectroscopy (PALS) (Ubbink et al., 2008; Ubbink, 2016).

The principal variables affecting the barrier properties of glassy carbohydrate matrices are temperature, water content and matrix formulation. Of particular importance is water, first and foremost as it is a strong plasticizer of amorphous carbohydrates, reducing the matrix T_g significantly (Roos, 1995). Secondly, in the glassy state, water impacts the molecular packing and the dynamics of amorphous carbohydrates via a complex mechanism where, depending on the concentration present, water may act as an antiplasticizer or plasticizer of the carbohydrate matrix (Ubbink, 2016). At low concentrations ($\lesssim$ 5 wt.% (Roussenova et al., 2010)), water acts as an antiplasticizer, lowering the matrix T_g but also reducing the average size of the free volume holes in the glassy state (Townrow et al., 2007; Roussenova, 2011). At higher concentrations, water acts as a plasticizer, continuing to reduce T_g of the matrix but increasing the average size of the free volume holes in the glassy state (Townrow et al., 2007). In this regime, water not only enhances its own molecular mobility (Tromp et al., 1997), but also of other small molecules (Schoonman et al., 2002; Gunning et al., 2000). The water content of carbohydrate-based glass encapsulation systems should therefore be as close to the so-called "antiplasticization threshold" as possible (Seow, 2010), as this minimizes the local free volume.

Low molecular weight matrix additives other than water have been shown to impact the molecular packing of glassy carbohydrates as well (Ubbink et al., 2008; Ubbink, 2016). Specifically, low molecular weight polyols, such as glycerol and sorbitol (Roussenova et al., 2010), and mono- and disaccharides such as

glucose and maltose (Kilburn et al., 2004, 2005; Townrow et al., 2007, 2010) act as antiplasticizers. These molecules reduce the average molecular hole size of glassy matrices consisting of intermediate and high molecular weight carbohydrates, such as starches and maltodextrins. The decrease in molecular hole size with increasing additive content corroborates findings from shelf-life testing (Kasapis et al., 2009; Ubbink, 2016).

Blends of starches or maltodextrins with low molecular weight polyols or mono- and disaccharides usually mix well at the molecular level and therefore consist of a single phase. Recently, however, it was observed that blends of flour and sucrose may show a limited degree of phase inhomogeneity, as witnessed by detailed modeling of the glass transitions as determined by differential scanning calorimetry (DSC) (Roudaut & Wallecan, 2015). To assume molecular miscibility of blend components may thus be incorrect. A more pronounced separation into two distinct phases was observed for blends of octenyl succinic anhydride-modified (OSA) starch and sucrose (Tedeschi et al., 2016).

The partial incompatibility of matrix components leads to a number of phenomena not observed for homogeneous systems. For some applications, such as the targeted release of pharmaceuticals, matrix incompatibility may be sought in order to produce two distinct phases with specific properties, one acting to impart stability during storage and the other to act as the "delivery vessel" (Tedeschi et al., 2016). Phase separation of the constituents of encapsulation matrices could however also lead to reduced barrier properties of glassy carbohydrate blends and is thus a vital property to consider and control in the development of matrix formulations (Tedeschi et al., 2016; Hughes et al., 2016).

In this study we first present the analysis of the glass transition behavior of the blends, as measured by DSC, as a function of composition and water content. Then, using ^{1}H low-resolution solid-state NMR, aspects of the matrix dynamics that are related to the phase behavior of the matrices. Finally, we introduce a model to quantify both the relative abundance of the phases present within the anhydrous blends and the composition of these phases. Our overarching aim is to provide a quantitative description of the phase behavior, matrix structure and

component dynamics in relation to the blend composition and thermodynamic parameters.

2. Experimental

2.1. Preparation of hydrophobically-modified starch (HMS) - sucrose (S) blends

HMS-S blends were prepared with well-defined ratios of HMS and S prior to water activity equilibration, with mass fractions of sucrose on anhydrous basis (Q'_S) of 0.10, 0.20, 0.40, 0.55 and 0.75 as expressed by:

$$Q'_S = \frac{m_S}{(m_S + m_{HMS})}, \tag{1}$$

where m_S and m_{HMS} are the mass of sucrose and HMS used in the anhydrous blend formulation, respectively. Structural parameters representative of the OSA starch, denoted here as hydrophobically modified starch, used in this study are a degree of branching (DOB) of 5.19 %, a degree of substitution (DOS) of 2.26 %, a hydrodynamic radius ($\langle R_h \rangle$) of 4.37 nm and a viscosity of 61.2 mPa·s. The DOB and DOS were determined by ^{1}H NMR at 298 K and $\langle R_h \rangle$ by size exclusion chromatography (SEC) at 298 K (Tizzotti et al., 2011). For the viscosity measurement, HMS was mixed with water (40 wt.% HMS) and shaken overnight at 348 K. The viscosity of the HMS in water was then measured at 348 K using a viscometer (NDJ-5S, Shanghai Changji Geology Co., Ltd, Shanghai). Sucrose (S) (from sugar cane) was purchased from Tate & Lyle PLC (London, UK). HMS-S blends were prepared using the following experimental protocol. Aqueous solutions of HMS and sucrose were prepared at $\sim$ 45 - 60 wt.% solids by stirring (at 400 rpm) precisely measured amounts of the ingredients in demineralized water for 2 hours at 360 K. The HMS-S solutions were then converted to amorphous powders in the glassy state by spray drying using a Mobile Minor 2000 spray-dryer (GEA, Denmark). After water activity equilibration, the water content on wet basis (Q_w) of the HMS-S blends is given by:

$$Q_w = \frac{m_w}{(m_C + m_w)}. \tag{2}$$

Here, m_w and m_C are the total masses of water and carbohydrates (m_S + m_{HMS}) in the blend, respectively.

2.2. Initial water content determination and water activity equilibration

Initial water contents of the HMS-S blends were determined by drying in a laboratory oven for 27 h at 353 K under a pressure below 25 mbar under a slight flow of dry nitrogen. The blends were then equilibrated at a range of water activities (a_w) at 298 K in desiccators containing saturated salt solutions (a_w (salt) = 0.11 (LiCl), 0.22 (CH_3COOK), 0.33 ($MgCl_2$), 0.43 (K_2CO_3), 0.54 ($Mg(NO_3)_2$), 0.75 (NaCl). The pure spray-dried HMS ($Q'_S = 0.0$) was also equilibrated at $a_w = 0.68$ (KI)) (Greenspan, 1977). Water sorption was followed gravimetrically for 1200 h. In this time, all samples reached their equilibrium water content.

Anhydrous HMS-S blends were prepared by oven drying at 318 K for 48 hrs then 72 hrs at 298 K followed by 48 hrs at 318 K, all under a reduced pressure of 5 mbar and a slight flow of dry nitrogen gas. Water activities of the dried samples were determined using a LabMASTER-aw (Novasina, Lachen, Switzerland).

2.3. Powder X-ray diffraction (XRD)

Powder diffraction patterns were collected using a Phillips X'pert Pro diffractometer (Panalytical) operating at 40 kV and 30 mA utilizing Cu K_α radiation ($\lambda = 0.154$ nm). Scans were performed at 298 K under local atmospheric humidity over the 2θ range 5-35° with a step size of 0.02° and a data acquisition time of 2 s at each step.

2.4. Differential scanning calorimetry (DSC)

DSC analyses were performed using a Discovery DSC equipped with a Discovery Liquid Nitrogen Pump Accessory (LN2P) from TA Instruments, Waters GmbH (Eschborn, Germany). Approximately 15 mg of water activity equilibrated sample was precisely weighted in a Tzero medium-pressure aluminum

pan (TA Instruments), which was subsequently hermetically sealed with a Tzero Hermetic Lid (TA Instruments). An empty pan with sealed lid was used as a reference. The instrument was calibrated with an indium standard and dry N_2 was passed through the DSC cell at a flow rate of 50 ml·min^{-1} during measurements. The samples were heated at a rate of 5 K·min^{-1} to 400 K (first heating run) and held at that temperature for 1 min. The samples were then cooled to 180 K at a rate of 20 K·min^{-1}, stabilized for 3 minutes at 180 K and reheated to 400 K at a rate of 5 K·min^{-1}(second heating run). All analyses of the sample glass transitions were performed using the thermograms obtained during the second heating ramp and converted to specific heat capacity (C_p).

Multiple glass transitions are resolved by modeling the DSC thermograms across a wide temperature range following a further development of the method by Roudaut *et al.* (Roudaut & Wallecan, 2015). This allows for the consistent treatment of data and provides confidence in the results obtained from the analysis. In our implementation, the first derivative of the specific heat capacity (dC_p/dT) across a single glass transition is modeled by a Gaussian line shape (G)(Song et al., 1997; Hourston et al., 1997, 1999). It then follows for n glass transitions, dC_p/dT may be expressed as:

$$\frac{dC_p}{dT} = \sum_{i=1}^{n} G_i + B, \tag{3}$$

where B approximates the contribution of the instrument baseline to the measured dC_p/dT and:

$$G_i = \frac{\Delta C_{p,i}}{\sigma_i \sqrt{2\pi}} \exp\left[-\frac{(T - T_{g,i})^2}{2\sigma_i^2}\right], \tag{4}$$

where T_g is the centre of the Gaussian (the transition mid-point), σ_i is standard deviation of the Gaussian, which is used to calculate the full width at half maximum of the transition ($\Delta T_{g,i} = \mathrm{FWHM}_i = 2\sqrt{2\ln 2}\ \sigma_i$), and $\Delta C_{p,i}$ is the change in specific heat capacity of the sample across the glass transition. The T_g obtained in this way may thus be identified as the $T_{g,midpoint}$.

An example of the analysis of the DSC data is presented in Figure 1, demonstrating that two overlapping glass transitions in the $Q'_S = 0.2$ blend equili-

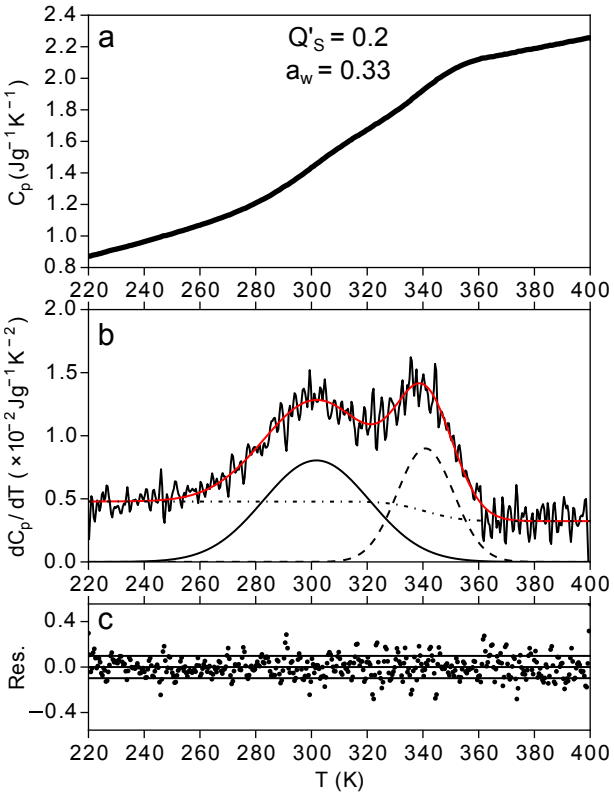

Figure 1: Example of the determination of overlapping glass transitions from **(a)** the DSC heat capacity (C_p) curve using **(b)** the first derivative (dC_p/dT) by the of fitting equation 4 (model fit indicated by solid red line) using two Gaussian curves (solid and dashed lines) upon a sigmoidal baseline (dash-dot-dash line). The lack of structure in the residuals **(c)** indicates the model describes the DSC data well. (For interpretation of the references to color in this figure legend, the reader is referred to the web version of this article.)

brated at $a_w = 0.33$ can be accurately resolved by two Gaussians upon a sigmoidal baseline ($B = \mathrm{erf}(T)$) in dC_p/dT, as indicated by structureless residuals. The number of Gaussians (corresponding to the number of glass transitions) was chosen to achieve both a satisfactory fit (structureless residuals as a function of temperature) and reproducible results when different initial parameter values were chosen. Either a constant or an error function was used to approximate B, the latter of which was utilized only when significant structure in the residuals existed before or after the completion of the glass transitions, which was found

to be the case in the low Q'_S (≤ 0.2) blends.

2.5. Solid-state NMR

Low-resolution ^{1}H solid-state NMR measurements were carried out on a spectrometer constituted of a Stelar PC-NMR system and a permanent magnet working at the ^{1}H Larmor frequency of 20.8 MHz, equipped with a Stelar 5 mm static probe and a Stelar VT system. ^{1}H Free Induction Decays (FIDs) were recorded in the temperature range 293-373 K on heating under on-resonance conditions by means of a solid echo pulse sequence. At least 256 transients were accumulated for each FID using an echo delay time of 12 μs and a relaxation delay of 2 s. The 90^o pulse duration was 3 μs. Temperature was controlled within $\pm$ 0.1 K.

In order to reproduce the experimental FIDs, nonlinear least-squares fittings were carried out using a linear combination of analytical functions commonly employed for this scope, chosen among exponential, Gaussian, Weibullian, Pake and Abragamian functions (Hansen et al., 1998). The linear combination of functions best reproducing the experimental FID was chosen on the basis of the Occam's Razor principle and of the minimization of the χ^2 of the fitting. The best results were obtained using a sum of one or two exponentials and a Pake function. The generic analytical function used in all cases can be written as:

$$S(t) = I_{E1} \cdot E1(t) + I_{E2} \cdot E2(t) + I_P \cdot P(t), \tag{5}$$

where $S(t)$ is normalized so to give $S(0) = 100$, I_i is the weight percentage of the i-type function (expressed in %), $E1$, $E2$ and P indicate the two exponential functions and the Pake function, respectively. The exponential functions:

$$E(t) = \exp(-t/T_2), \tag{6}$$

are characterized by the spin-spin relaxation time T_2, while the Pake function, derived as the inverse Fourier transform of the original expression in the frequency domain (Pake, 1948), can be written as (Look et al., 1966):

$$P(t) = \sqrt{\frac{\pi}{6}} \exp\left(-\frac{\beta^2 t^2}{2}\right) \left[\frac{\cos \alpha t}{\sqrt{\alpha t}} C\sqrt{\frac{6\alpha t}{\pi}} + \frac{\sin \alpha t}{\sqrt{\alpha t}} S\sqrt{\frac{6\alpha t}{\pi}}\right], \tag{7}$$

where C and S are approximated Fresnel functions (Abramowitz & Stegun, 1970), $\alpha = 3\gamma^2\hbar/4R_{HH}^3$, and γ is the proton gyromagnetic ratio. The Pake function is therefore characterized by the parameters R_{HH} and β, which respectively represent the distance between two nearest neighbor protons and the width of the Gaussian line due to the dipolar interactions between non-nearest neighbor protons. After having verified that the parameter β did not vary significantly from sample to sample and at different temperatures, it was kept fixed to a value of 50 kHz in the final fittings in order to reduce the correlation among the fitting parameters. All HMS-S blends studied with solid-state NMR were equilibrated at $a_w = 0.22$ at 298 K.

3. Results and Discussion

3.1. X-ray diffraction

Following spray drying and subsequent water activity equilibration, all blends were confirmed to be completely amorphous by X-ray scattering (Ubbink et al., 2018). Even at high water activities and sucrose contents, there is no evidence of sucrose crystallinity. Considering that amorphous sucrose in the rubbery state has been shown to crystallize on the timescale of a few days or less (Makower & Dye, 1956), which is far shorter than the a_w equilibration timescales used here, the absence of crystalline peaks in the diffraction patterns implies that the presence of the HMS is inhibiting the crystallization of the sucrose. In agreement with findings on related systems (Saleki-Gerhardt & Zografi, 1994; Chirife & Inglesias, 1978; te Booy et al., 1992).

3.2. Differential Scanning Calorimetry (DSC)

Second heating DSC thermograms for the HMS-S blends equilibrated at $a_w = 0.33$ and $Q'_S = 0.4$ blends equilibrated at all a_w are shown in Figures 2(a) and 2(b), respectively. For the $Q'_S = 0.4$ blends, at $a_w = 0.11$ there appears to be a single, wide transition. This single "step" representing the change in the specific heat capacity (ΔC_p) of the system that occurs as T_g is crossed. At

higher values of a_w (0.22 and 0.33) this step appears with a "tail" extending to higher temperatures, suggesting a transition width of $\sim$ 80 K. This may be taken as an indication of an underlying second transition, as the width of the glass transition is commonly significantly narrower ($\sim$ 10 - 30 K) in carbohydrate polymers (Roos, 1995). At the highest water activities (a_w = 0.43, 0.54 and 0.75), two separate glass transitions become clearly visible.

It was found that for all HMS-S blends dC_p/dT could be accurately modeled assuming two transitions ($n = 2$ in Eq. 3) with the exception of the $Q'_S = 0.2$ blend equilibrated at $a_w = 0.75$, for which an intermediate third transition was resolved. Fitted transition parameters for the hydrated an oven-dried blends are presented in Ubbink et al. (2018). The presence of two resolvable glass transitions in all HMS-S blends indicates the presence of two distinct amorphous phases. The dependence of the upper ($T_{g,upper}$, higher temperature) and lower ($T_{g,lower}$, lower temperature) T_g values on the total water content (Q_w) of the blends are presented in Figures 3(a) and 3(b), respectively.

In order to discuss the behavior of the blend T_g values, it is necessary to first discuss the Q_w dependence of the T_g values of the blend components, namely the HMS ($T_{g,HMS}$) and sucrose ($T_{g,S}$).

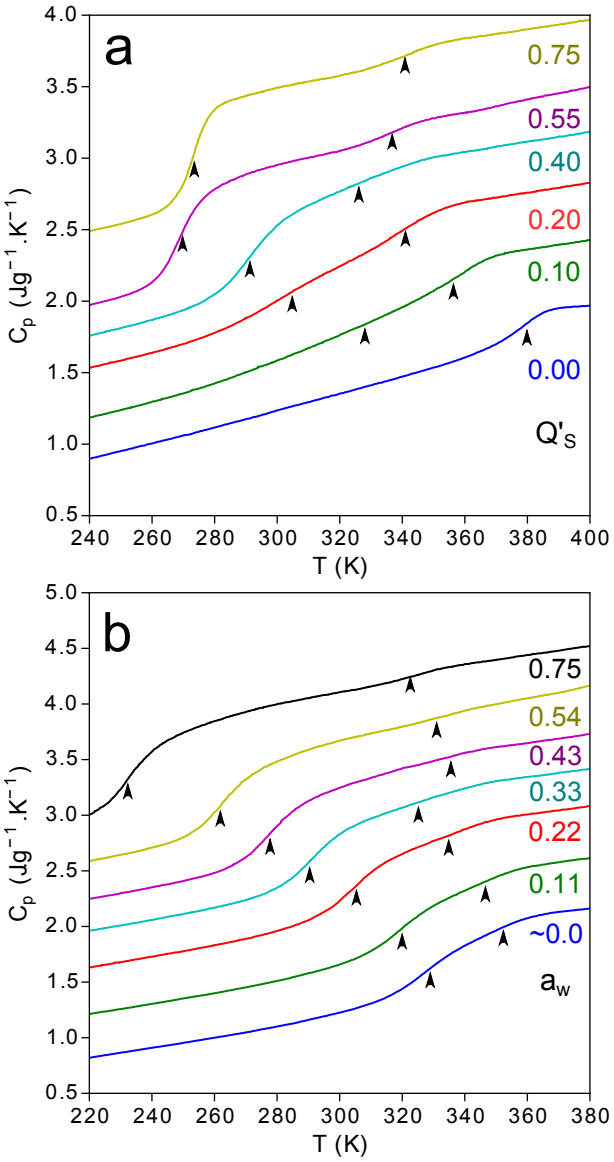

Figure 2: DSC second heating scans for HMS-S blends **(a)** equilibrated at $a_w = 0.33$ with sucrose weight fraction on anhydrous blend basis $Q'_S = 0.00$ (blue), 0.10 (green), 0.20 (red), 0.40 (cyan), 0.55 (magenta) and 0.75 (yellow), and **(b)** for $Q'_S = 0.2$ blends equilibrated at $a_w \sim 0.0$ (blue), 0.11 (green), 0.22 (red), 0.33 (cyan), 0.43 (magenta), 0.54 (yellow) and 0.75 (black). The arrows indicate the positions of the resolved values of T_g, determined as outlined in Section 2.4. (For interpretation of the references to color in this figure legend, the reader is referred to the web version of this article.)

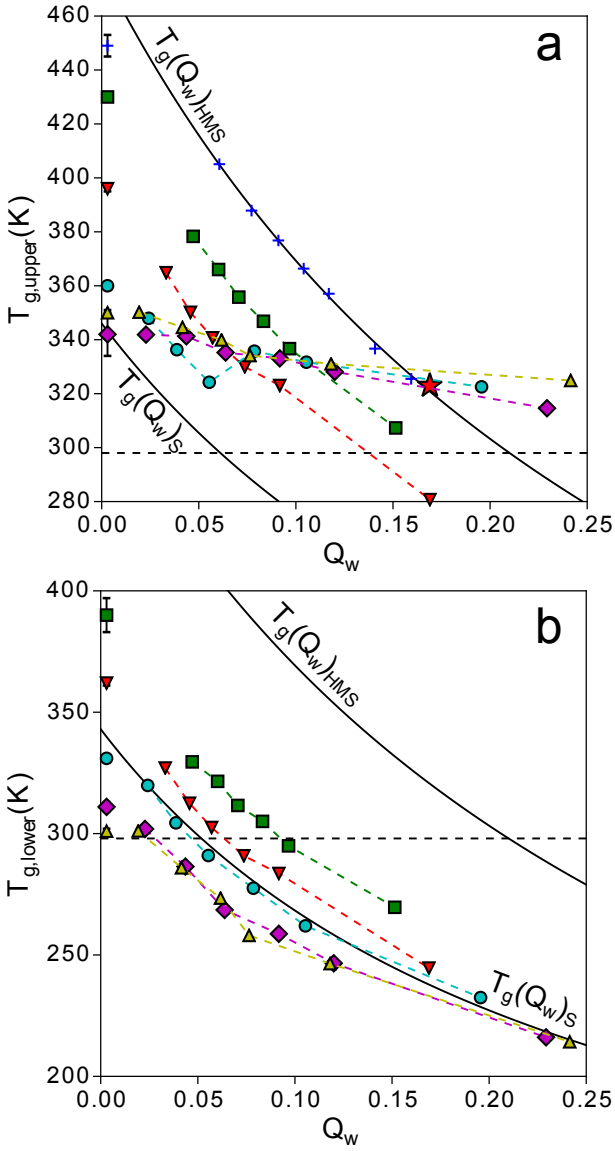

Figure 3: **(a)** Lower ($T_{g,lower}$) and **(b)** upper ($T_{g,upper}$) glass transition temperatures for the HMS-S blends with $Q'_S = 0.00$ (blue crosses), 0.1 (green squares), 0.2 (red inverted triangles), 0.4 (cyan circles), 0.55 (magenta diamonds) and 0.75 (yellow triangles) as a function of water content of the blends, Q_w. The red star indicates the intermediate glass transition resolved for the $Q'_S = 0.2$ blend equilibrated at $a_w = 0.75$. The oven-dried blends are plotted at $Q_w = 0.005$. The solid black lines represent the GT fits for pure HMS ($T_g(Q_w)_{HMS}$) and sucrose ($T_g(Q_w)_S$). The horizontal dashed line indicates $T = 298$ K. (For interpretation of the references to color in this figure legend, the reader is referred to the web version of this article.)

A number of models have been developed to analyze the plasticization of amorphous polymers by water and other low molecular weight compounds (Fox, 1956; Kwei, 1984; Couchman & Karasz, 1978; Gordon & Taylor, 1952). All of these models were derived based on the assumptions that the matrix components are miscible at the molecular level and that the properties of the matrix components are additive in terms of the volume fractions they occupy of the overall matrix. In particular the latter assumption is likely to be invalid for carbohydrate-water systems (Ubbink et al., 2007). Notwithstanding, most models fit the plasticization of carbohydrates by water fairly well. Here, we use the Gordon-Taylor (GT) equation for a binary blend of a carbohydrate and water to model the dependence of T_g on Q_w in HMS and sucrose. The GT equation may be expressed in the form (Gordon & Taylor, 1952):

$$T_g = \frac{Q_C T_{g,C} + k_{GT} Q_w T_{g,w}}{Q_C + k_{GT} Q_w}, \tag{8}$$

where $T_{g,w}$ is the glass transition temperature of super-cooled water, commonly taken as $T_{g,w} = 136$ K (Roos, 1995). $T_{g,C}$ and k_{GT}, are the glass transition temperature of the anhydrous carbohydrate matrix and the GT coefficient, respectively. Both $T_{g,C}$ and k_{GT} are considered as fitting parameters in the least-squares fitting of the GT equation to experimentally determined values of T_g.

The solid black lines in Figure 3 indicate the GT fits to the water content series of pure HMS (upper line) and sucrose (lower line). The GT values for sucrose were taken from previous studies: $T_{g,S} = 343$ K and $k_{GT} = 5.1$ (Blond et al., 1997; Frank, 2007). The higher value of k_{GT} for the sucrose compared to HMS suggests that water has a somewhat greater plasticizing effect for sucrose than HMS.

There is significant variation in experimental values for $T_{g,S}$ reported in various sources (reviewed by Frank (2007)). We have used a value for $T_{g,S}$, which was determined using a similar DSC protocol as in the present investigation. For the HMS, the GT fitting returned $T_{g,HMS} = 477$ K and $k_{GT} = 4.2$. The T_g for the oven-dried HMS was omitted in this fitting as from Ubbink et al. (2018) it is seen that the sample contains some residual water. Our experimental value

for $T_{g,HMS}$ is $\sim$ 20 K lower than the T_g reported for anhydrous amylopectin (Kalichevsky et al., 1993; Kalichevsky & Blanshard, 1993; Kalichevsky et al., 1992). This is due to both the average number of hydroxyl groups per glucose ring that may participate in hydrogen bonding (as some are replaced by OSA) being lower, and a reduction in the efficiency of hydrogen bonding as the rather bulky OSA groups decrease the density of molecular packing (Silaket et al., 2014). The combined effects hinder the formation of the strong hydrogen bonding interactions that give rise to the high T_g value of starches (Ubbink et al., 2008; van der Sman, 2013).

$T_{g,lower}$ decreases with water content for all blend compositions (Figure 3(b)), as expected for materials that are plasticized by water. As the sucrose content of the blends increases, the lower glass transition temperature approaches and then surpasses the T_g line of pure sucrose (Figure 3(b)). In particular for the blends with the highest sucrose contents (Q'_S = 0.55 and 0.75), the $T_{g,lower}$ values of the blends appear to fall below those of pure sucrose. There are two main considerations to be made to rationalize and understand this behavior, both of which are outlined below.

It is important to point out that the values of Q_w against which $T_{g,lower}$ and $T_{g,upper}$ are plotted represent the water content of the entire HMS-S matrix. Whilst the water activity of the blends is constant, the water content of the individual phases may vary considerably.

Figure 4(a) shows $T_{g,upper}$ and $T_{g,lower}$ of the Q'_S = 0.4 blend, highlighting the change in the behavior of the $T_{g,upper}$ with Q_w as $T_{g,lower}$ passes through 298 K (shown as the horizontal dashed line, corresponding to $Q_w \sim 0.05$). At the same point there is also a change in the behavior of ΔC_p as shown in Figure 4(b), the ΔC_p associated with $T_{g,lower}$ showing a large increase while that associated with $T_{g,lower}$ decreases. As these changes directly mirror the ΔC_p across the glass transition, one may infer compositional changes of the two phases from ΔC_p by considering ΔC_p for the raw components. For sucrose and water, ΔC_p may be taken as 0.76 and 1.94 $\mathrm{Jg^{-1}K^{-1}}$ respectively (Kalichevsky et al., 1992). For pure anhydrous HMS ΔC_p is assumed the same as for starch

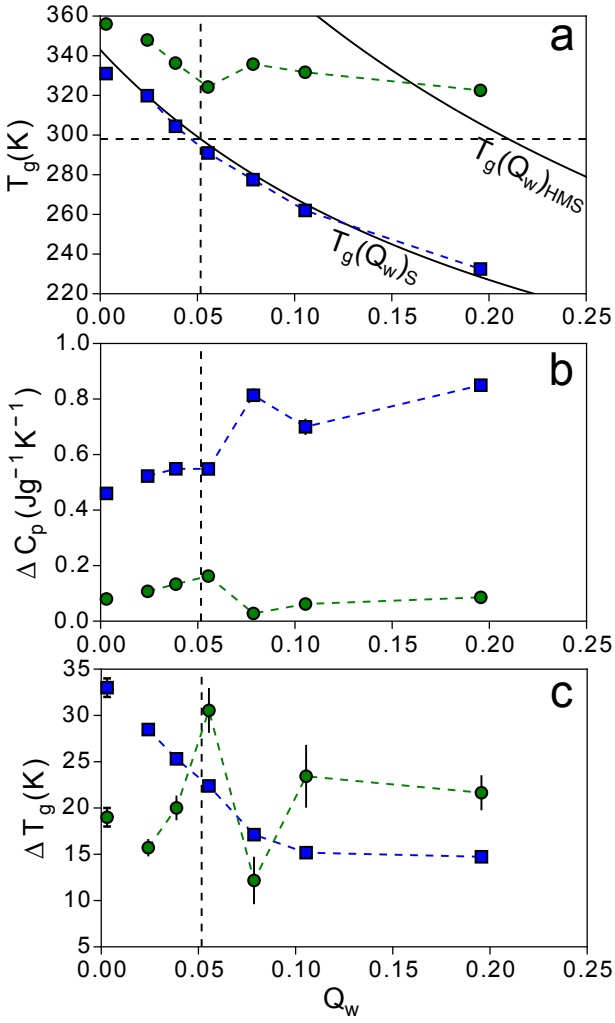

Figure 4: Parameters for the upper (green circles) and lower (blue circles) glass transition resolved for the $Q'_S = 0.4$ HMS-S blends. **(a)** The transition mid-point, T_g. **(b)** The change in specific heat capacity across the transition, ΔC_p. **(c)** The full width at half maximum of the transition, ΔT_g in dC_p/dT. As the Q_w of the dried blends has not been determined, results at low Q_w are only indicative. The horizontal dashed line in **(a)** indicates $T = 298K$ and the vertical dashed line indicates the value of Q_w at which $T_{g,lower}$ appears to fall below 298 K. (For interpretation of the references to color in this figure legend, the reader is referred to the web version of this article.)

(0.47 $Jg^{-1}K^{-1}$ (Orford et al., 1989; Kalichevsky et al., 1992)), giving $\Delta C_{p,w} > \Delta C_{p,S} > \Delta C_{p,HMS}$. At a fixed Q'_S one may expect a simple linear increase in the fitted ΔC_p values for increasing Q_w (approximating linear additivity of the ΔC_p values for the components within each phase). For the $Q'_S = 0.4$ blends there is a slight increase in ΔC_p for both transitions up to $Q_w \sim 0.05$, where there is a sudden increase in $\Delta C_{p,lower}$ and a decrease in $\Delta C_{p,upper}$ which we interpret as a sudden change in phase composition between samples. We suggest that when the sucrose-rich phase is in the rubbery state at 298 K post a_w equilibration, there is a migration of water and/or sucrose from the HMS-rich phase to the sucrose-rich phase resulting in $T_{g,upper}$ apparently lying above that expected for the pure HMS at the same value of Q_w, due to the loss of plasticizer from the phase (*i.e.* the plotted value of Q_w does not represent the true Q_w of the phase). This is confirmed by the sudden increase in $\Delta T_{g,upper}$.

Similar trends are seen for all transition parameters associated with both $T_{g,upper}$ and $T_{g,lower}$ in the a_w series at $Q'_S = 0.4$ (see Figure 5), indicating that changes in phase composition take place as $T_{g,lower}$ passes below 298 K. An additional feature to notice is the dependence of $\Delta T_{g,lower}$ on Q'_S. For low values of Q'_S, $\Delta T_{g,lower}$ is very wide, narrowing as Q'_S increases indicating that the sucrose-rich phase is becoming increasingly well defined with increasing sucrose content.

We infer that the water content of the sucrose-rich phase in the two-phase blends may become higher upon heating than the equivalent single-phase sucrose system. During initial heating, for example in the DSC, the sucrose-rich phase becomes rubbery. Then, at a temperature slightly above $T_{g,lower}$, this phase becomes ergodic, dramatically impacting the thermodynamics of water in the system. While in the glassy matrix, water binds to the quenched carbohydrate molecules via a mechanism involving both hydrogen bonding and matrix free volume, in the rubbery state, the thermodynamic state of water is determined by the entropy of mixing of the carbohydrate and water molecules (Ubbink et al., 2007). As a result, the chemical potential of water in the sucrose-rich phase suddenly drops when upon heating the phase becomes rubbery. From

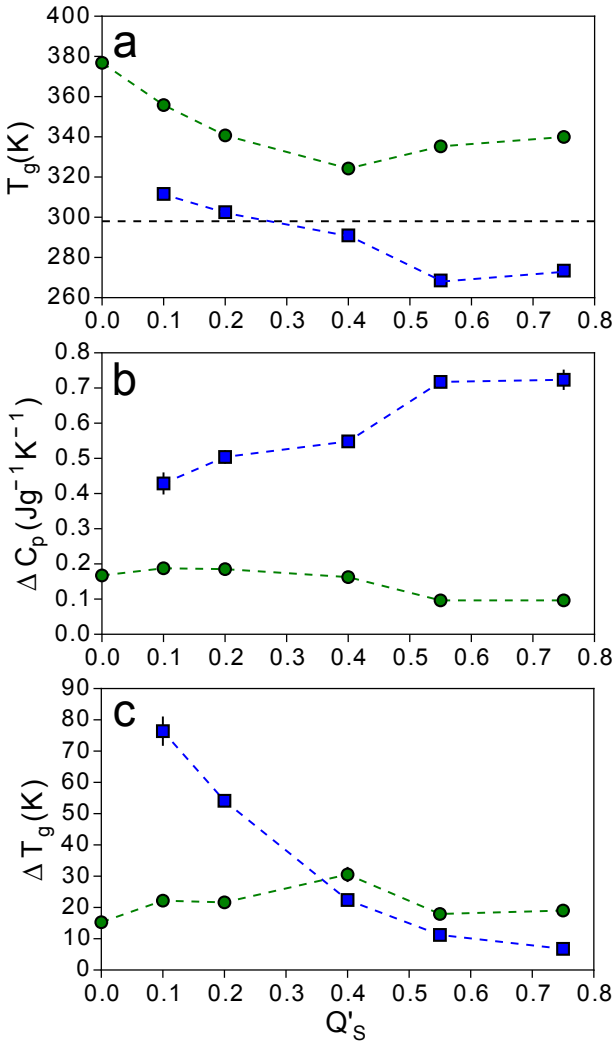

Figure 5: Parameters for the upper (green circles) and lower (blue circles) glass transition resolved for the $a_w = 0.33$ HMS-S blends and the pure HMS. **(a)** The transition mid-point, T_g. **(b)** The change in specific heat capacity across the transition, ΔC_p. **(c)** The full width at half maximum of the transition, ΔT_g in dC_p/dT. The horizontal dashed line in **(a)** indicates $T = 298$ K. (For interpretation of the references to color in this figure legend, the reader is referred to the web version of this article.)

a situation of dynamic water equilibrium between the two phases, we are now confronted by a significant difference in chemical potential of water between

the two phases, resulting in the net migration of water from the HMS-rich phase to the sucrose-rich phase. This is supported by previous observations on the temperature dependence of water sorption by starch, where increased water activity equilibration temperatures result in lower water contents for high amylopectin starch (Al-Muhtaseb et al., 2004).

3.3. ^1H Free Induction Decay (FID) Analysis

For the pure HMS and HMS-S blends containing up to $Q'_S = 0.4$ the ^{1}H on-resonance FIDs recorded at all temperatures could be accurately described as a sum of a single Pake function (with intensity I_{Pake}) and a single decaying exponential ($E1$, with intensity I_{E1} and decay constant $T_{2,E1} \sim$ 30-150 μs), analogous to an approach previously reported by G. Roudaut *et al.* (Roudaut et al., 2009) where the empirical Abragamian function was used in the place of the Pake function to model the ^{1}H FID of amorphous freeze-dried starch-sucrose blends. The P and $E1$ functions can be associated to protons in rigid/restricted mobility and mobile environments, respectively. Indeed, in the solid state, ^{1}H spin-spin relaxation is mainly determined by the strong dipolar couplings among the protons; molecular motions with frequencies higher than tens of kHz are effective in reducing such dipolar couplings, with a progressive increase of ^{1}H T_2 by increasing the degree of mobility. For the $Q'_S = 0.55$ and 0.75 blends, a second decaying exponential ($E2$, with intensity I_{E2} and decay constant $T_{2,E2} \sim$ 150-2000 μs) had to be added to the fitting function, indicating the presence of an additional distinguishable region of the sample, characterized by a larger degree of molecular mobility.

Firstly, by considering the temperature dependence of the intensities of the Pake and exponential functions shown in Figure 6, it is possible to comment upon the relative abundance of the phases with significantly different mobilities. The temperature dependence of I_{Pake} shown in Figure 6(a) shows little variation in the temperature range studied for the low Q'_S (< 0.4) HMS-S blends. For the pure HMS, the T_g lies above the temperature range studied, and therefore it is unexpected that any significant changes to the dynamics of the sample

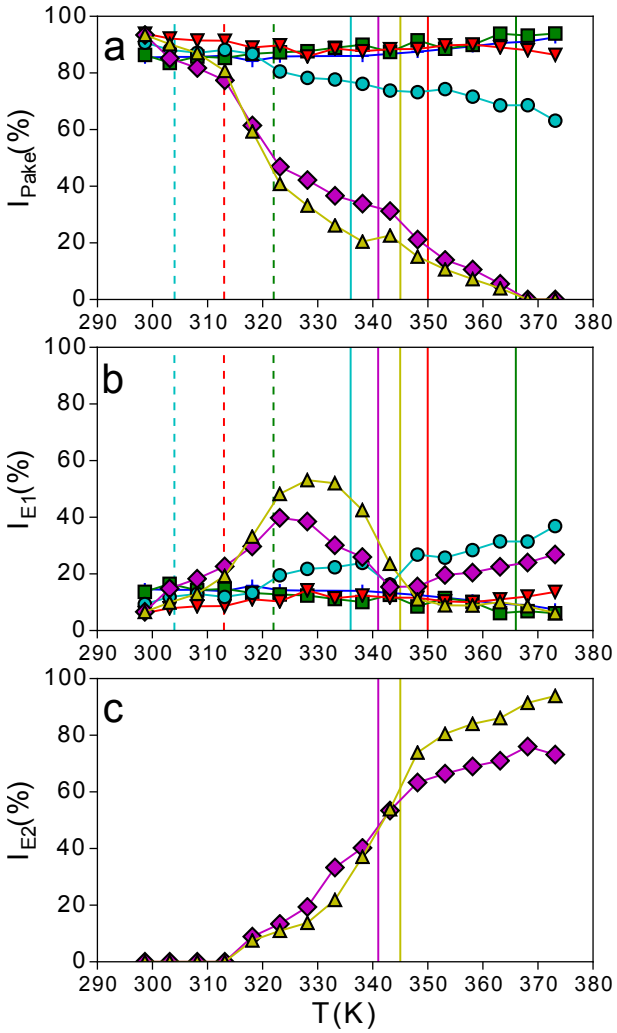

Figure 6: Intensities of the **(a)** Pake, **(b)** 1st exponential (E1) and **(c)** 2nd exponential (E2) functions used to model the FID spectra of the HMS-S blends equilibrated at $a_w = 0.22$ with $Q'_S = 0.00$ (blue crosses), 0.1 (green squares), 0.2 (red inverted triangles), 0.4 (cyan circles), 0.55 (magenta diamonds) and 0.75 (yellow triangles). The solid vertical lines indicate $T_{g,upper}$ and the dashed vertical lines $T_{g,lower}$ as determined by DSC. Note that the $T_{g,lower}$ of samples with $Q'_S = 0.55$ and 0.75 falls at temperatures lower than the investigated range. (For interpretation of the references to color in this figure legend, the reader is referred to the web version of this article.)

will occur. Even with this consideration, there is a small contribution to the FID from protons in slightly more mobile environments, which may arise from a local plasticization induced by water molecules. As the temperature is increased, I_{Pake} shows an unexpected slight increase and I_{E1} a corresponding decrease, which should be due to the loss of water from the sample by evaporation within the NMR tube. The behavior of the $Q'_S = 0.1$ and 0.2 blends show little difference from the pure HMS, indicating that the small sucrose-rich fractions, embedded in the HMS matrix, are still quite rigid.

The $Q'_S = 0.4$ blend shows the first sign of deviation from this behavior, exhibiting a steady decrease in I_{Pake} by increasing the temperature, with a corresponding increase of the mobile fraction of the blend (I_{E1}). This onset of mobility occurs between $T_{g,lower}$ and $T_{g,upper}$ of the blend, indicated by the dashed and solid cyan lines in Figure 6, respectively, and should be therefore be related to the glass-rubbery transition of sucrose-rich domains. It is worth noting that the increase in T_2 (and therefore, in this case, the passage from the Pake to the $E1$ behavior) is expected to occur a few tens of degrees above the calorimetric T_g, when the molecular motions reach a correlation time of the order of some tens of ms, corresponding to the inverse of the dipolar field strength (a few tens of kHz).

The fraction of protons passing from the P to the $E1$ fractions between $T_{g,lower}$ and $T_{g,upper}$ is $\sim$ 13 %. Consequently, most of the sucrose is in a rigid environment even $\sim$ 20 K above $T_{g,lower}$.[1] By far the largest changes in the intensities of the Pake and exponentials are present in the high sucrose samples with $Q'_S = 0.55$ and 0.75. For these two samples I_{Pake} decreases by $\sim$ 50 and 70 %, respectively, when the temperature of the samples is increased from the lower to the upper T_g as measured by DSC. There is a close correspondence

[1] It must be noticed that Q'_S is the weight fraction of sucrose, while the weights determined by ^{1}H FID analysis must be compared with the fraction of sucrose ^{1}H nuclei. However, the two quantities almost coincide, due to the very similar percentage of hydrogen in sucrose and HMS.

between the fractional decrease in I_{Pake} and the sucrose content of the two blends ($Q'_S = 0.55$ and 0.75), which could be interpreted as all of the sucrose becoming mobile in this temperature interval. This is unlikely however, as the sucrose is distributed over the two phases, as is the modified starch. We rather interpret the decrease in I_{Pake} as related to the total fraction of mobile protons of both the sucrose and the starch.

A salient feature of the two highest sucrose content samples is the occurrence of a third, highly mobile phase, represented by $E2$. This phase becomes resolvable about 20-30 K below $T_{g,upper}$ for the two high sucrose blends ($Q'_S = 0.55$ and 0.75). The fraction of these highly mobile protons increases with increasing sucrose content, suggesting that these highly mobile protons are related to the sucrose rich phase. This is in agreement with the DSC results.

It is worth stressing that the distinction into these three dynamically distinguishable phases is not "static", nor simply associated to the glass transition temperatures of the matrices, but strictly dependent on the available thermal energy and thus to a specific relaxation time. P, $E1$ and $E2$ domains can therefore not be assigned to specific, fixed domains within the samples. The interpretation is rather that these different dynamic phases progressively transform from one into another as a function of temperature. While the fractions of the P and $E2$ dynamic phases monotonically decrease and increase, respectively, with increasing temperature, the $E1$ dynamic phase exhibits a more complex behavior. For all samples, the fraction of the $E1$ phase increases as the fraction of the P dynamic phase decreases. For the two samples highest in sucrose part of the $E1$ fraction transforms into the even more mobile $E2$ fraction. Moreover, as shown in Figure 7, the spin-lattice relaxation time T_2 continuously increases with temperature for $E2$ fraction, with the slope becoming steeper above $T_{g,upper}$ of the samples. This increase in T_2 signifies a progressive increase of the mobility of the $E2$ fraction.

The temperature dependence of T_2 of the $E1$ fraction is more complex and difficult to be rationalized: its behavior can be possibly justified in the context of the above mentioned dynamic transformation among the different fractions,

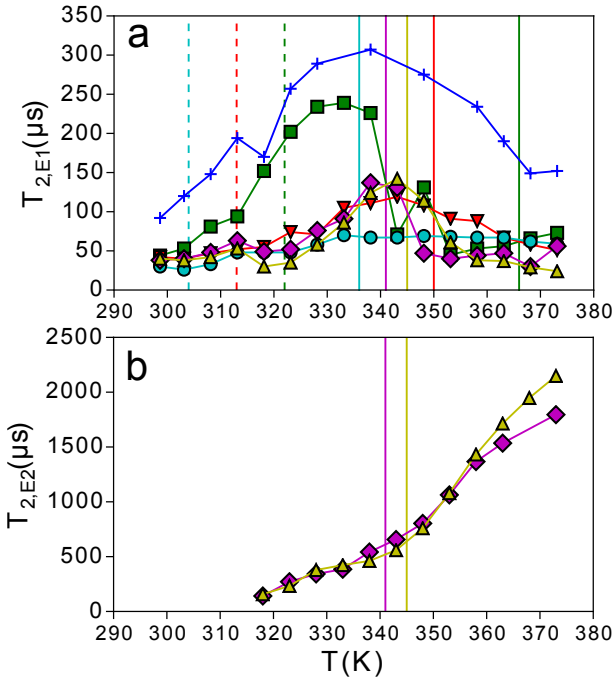

Figure 7: Characteristic relaxation times of **(a)** the 1st exponential (E1) and **(b)** 2nd exponential (E2) functions used to model the FID spectra of the HMS-S blends equilibrated at $a_w = 0.22$ with $Q'_S = 0.00$ (blue crosses), 0.1 (green squares), 0.2 (red inverted triangles), 0.4 (cyan circles), 0.55 (magenta diamonds) and 0.75 (yellow triangles). The solid vertical lines indicate $T_{g,upper}$ and the dashed vertical lines $T_{g,lower}$ as determined by DSC. Note that the $T_{g,lower}$ of samples with $Q'_S = 0.55$ and 0.75 lies at temperatures lower than the investigated range. (For interpretation of the references to color in this figure legend, the reader is referred to the web version of this article.)

as observed previously by Roudaut *et al.*(Roudaut et al., 2009).

3.4. Phase composition modeling

The experimental $T_{g,i}$ (where i = *upper* or *lower* for the HMS-rich and sucrose-rich phases, respectively) values obtained by DSC are here used to estimate the HMS and sucrose contents of the two phases present in selected blends. By fitting the GT model (Equation 8) to both $T_{g,upper}$ and $T_{g,lower}$ values of

Table 1: Parameters obtained for the fitting of $T_{g,upper}$ (u) and $T_{g,lower}$ (l) to the Gordon-Taylor equation (Equation 8) for the hydrated HMS-S blends. The a_w range indicates the equilibration water activities for which the samples are entirely in the glassy state at 298 K (*i.e.* $T_{g,lower} > 298K$). Q'_S is the sucrose mass fraction for the entire anhydrous blend.

Q'_S (u/l)	a_w range	$T_{g,C}$ (K)	k_{GT}
0.0	0.11-0.75	477±4	4.2±0.1
0.1 (u)	0.11-0.54	435±2	4.6±0.1
0.1 (l)	0.11-0.54	422±7	6.6±0.5
0.2 (u)	0.11-0.43	409±7	5.4±0.6
0.2 (l)	0.11-0.43	396±16	9.0±1.7
0.4 (u)	0.11-0.33	371±4	4.4±0.4
0.4 (l)	0.11-0.33	349±1	6.4±0.2
1.0[a]	n/a	343	5.1

[a]Values for pure amorphous sucrose taken from Frank (2007).

each blend over a sample-specific Q_w range, the anhydrous $T_{g,C}$ for each phase may be estimated. The sample-specific Q_w range over which T_g fitting is performed is chosen under the assumption that the composition of the phases in terms of HMS and sucrose is constant (*i.e.* a change in Q_w does not alter the ratio of HMS:S in each phase). Due to the apparent redistribution of phase components for matrices existing in the partially rubbery state at or below the a_w equilibration temperature of 298 K (see Section 3.2), only $T_{g,i}$ values are used in the fitting if they lie above 298 K, or in other words, for blends that are entirely glassy at 298 K. The HMS-S blends for which this condition is satisfied are presented in Table 1, along with the resulting parameters obtained from the GT fit. We utilize the values of $T_{g,C}$ from the GT fitting rather than the experimentally determined $T_{g,i}$ values for the oven-dried HMS-S blends as some residual moisture remains (see Ubbink et al. (2018)).

With the values of $T_{g,C}$ of the anhydrous binary HMS-S blend phases estimated, it is possible to construct a "master" GT curve for sucrose in HMS,

which is written:

$$T_{g,C} = \frac{Q_{HMS}T_{g,HMS} + k_{GT}Q_S T_{g,S}}{Q_{HMS} + k_{GT}Q_S}, \tag{9}$$

where Q_{HMS} and Q_S are the mass fractions of HMS and sucrose in the binary phase with glass transition temperature $T_{g,C}$. As values of $T_{g,C}$ have been estimated and anhydrous values of $T_{g,HMS}$ and $T_{g,S}$ are known (see Table 1), it is possible to determine Q_{HMS}, Q_S and k_{GT} by least squares minimization between the model curve (Equation 9) and the T_g's while conserving the total mass of both sucrose and HMS available to the phases. In other words, the mass of HMS and sucrose in each phase is allowed to fluctuate during the optimization, but is constrained by the total mass of sucrose and HMS in each blend and all T_g values being fixed. This method therefore allows one to estimate the composition of each anhydrous phase in the blends to be extracted along with the mass of each phase, m_{lower} and m_{upper} for the sucrose and HMS-rich phases respectively (presented as per 100 g of sample).

Our model, the results for which are presented in part (a) of Table 2 and shown graphically in Figure 8, shows that as the total sucrose content of the blend increases, both the mass fraction and sucrose content of the HMS-rich phase increase, whereas the mass fraction of the sucrose-rich phase decreases with increasing sucrose content. At the same time, the composition of the sucrose-rich phase steadily converges towards a pure sucrose phase. The mass fraction the sucrose-rich phase (m_{lower}) might seem low (see results (a) in Table 2). However, it is observed that the mass balance between the phases is sensitively dependent on the model parameters, especially for the $Q'_S = 0.4$ blend. Taking for instance an alternative value of 338 K for $T_{g,S}$, results in an increase of m_{lower} from 3 wt.% to 15 wt.% for the blend with $Q'_S = 0.4$ (see results (b) in Table 2). This latter value matches well with the results from the variable temperature ^{1}H FID solid-state NMR experiments presented in Section 3.3, which showed that the vicinity of $T_{g,lower}$ in the $Q'_S = 0.4$ blend, a population of protons with distinctly increased mobility existed with a relative abundance

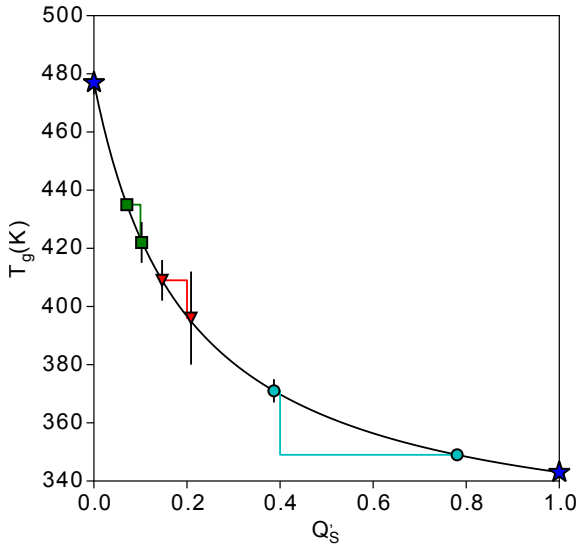

Figure 8: Optimized ("Master") GT model fit (solid black curve) for anhydrous HMS-S blends with Q'_S(of the entire anhydrous matrix) = 0.1 (green), 0.2 (red), 0.4 (cyan) giving $k_{GT} \approx 5.5$. Blue stars indicate the T_g values of anhydrous HMS and sucrose. The curve is constructed using parameters in Table 1. The vertical colored lines indicate the values of Q'_S that would represent ideal molecular mixing of HMS and sucrose (*i.e.* the composition expected for a homogeneous single-phase blend) and the horizontal colored lines highlight the deviation from this behavior. (For interpretation of the references to color in this figure legend, the reader is referred to the web version of this article.)

of $\sim$ 15-20 %.

4. Conclusions

A detailed analysis of the differential specific heat capacity curves from differential scanning calorimetry demonstrates that a significant degree of phase separation occurs in amorphous blends of HMS and sucrose, as indicated by the presence of multiple distinct glass transitions. It turns out that one of the phases is enriched in HMS and the other is enriched in sucrose, with the composition of the phases depending on the blend ratio between HMS and sucrose. The phase separation is confirmed by solid state NMR, which furthermore shows that the dynamics in the HMS-S blends with up to 40 wt.% sucrose are characterized

Table 2: Sucrose content ($Q'_{S,lower/upper}$) and mass per 100g of HMS-S blend ($m_{lower/upper}$) of the sucrose-rich (lower) and the HMS-rich (upper) phases for the anhydrous HMS-S blends returned in the construction of the anhydrous GT master curve using **(a)** $T_{g,HMS} = 477$ K, $T_{g,S} = 343$ K (optimal value of $k_{GT} \approx 5.5$) and **(b)** $T_{g,HMS} = 477$ K, $T_{g,S} = 338$ K (optimal value of $k_{GT} \approx 5.9$).

Q'_S (sample)	$T_{g,lower}$ (K)	$Q'_{S,lower}$ $\times 10^{-2}$	m_{lower} (g / 100 g)	$T_{g,upper}$ (K)	$Q'_{S,upper}$ $\times 10^{-2}$	m_{upper} (g / 100 g)
(a)						
0.1	422 ± 7	11.4	61.7	435 ± 2	7.7	38.3
0.2	396 ± 16	21.8	69.8	409 ± 7	15.8	30.2
0.4	349 ± 1	79.6	2.9	371 ± 4	38.8	97.1
(b)						
0.1	422 ± 7	10.2	95.3	435 ± 2	6.9	4.7
0.2	396 ± 16	22.3	70.4	409 ± 7	14.5	29.6
0.4	349 ± 1	66.5	15.0	371 ± 4	35.3	85.0

by a rigid phase and a mobile phase; the fraction of the mobile phase becoming significant when the sucrose-rich phase passes through the glass transition. The two blends highest in sucrose (55 wt.% and 75 wt.%) in addition show a third, highly mobile phase, which may be transient in nature. The presence of two phases leads to a dynamic compositional behavior with respect to water transfer and plasticization, the sucrose-rich phase becoming ergodic at a temperature slightly above the glass transition temperature and the water content of the phase being governed by the mixing entropy of the phase. It is suggested that this leads to a transfer of water from the HMS-rich phase to the sucrose-rich phase, resulting in a significant increase of the T_g of the HMS-rich phase and a decrease of the T_g of the sucrose-rich phase. The timescale at which this process occurs is currently unknown and requires further investigation. We have introduced a quantitative model allowing the prediction of the phase compositions based on the assumption that the dependence of the T_g on the composition is

the same for both the HMS-rich phase and the sucrose-rich phase. The model predicts that, with increasing sucrose content, the weight fraction of the sucrose-rich phase decreases, while the sucrose content in both the HMS-rich phase and the sucrose-rich phase increases. Furthermore, the relative abundance of the sucrose-rich phase decreases as the matrix sucrose content increases, a result mirrored by the relative population of highly mobile protons detected by ^{1}H FID solid-state NMR experiments. Our results indicate that many matrices of relevance to food, pharmaceutics and encapsulation show significant degrees of matrix heterogeneity, most likely originating in phase separation. This may give rise to a range of static and dynamic properties of such matrices that are hitherto unexplored but that may have a major impact on stability and performance.

Acknowledgements:

We thank Rob Richardson (University of Bristol) for the use of the X-ray diffractometer the University of Bristol. DSM Nutritional Products AG is thanked for the financial support of this work. We also acknowledge financial support from EPSRC (Ref: EP/J500379/1).

References

Abramowitz, M. & Stegun, I. A. (Eds.). (1970). *Handbook of Mathematical Functions with Formulas, Graphs and Mathematical Tables.* (9th ed.). Dover Publications, Inc., New York.

Al-Muhtaseb, A., McMinn, W., & Magee, T. (2004). Water sorption isotherms of starch powders: Part 1: Mathematical description of experimental data. *Journal of Food Engineering*, *61*(3), 297–307.

Blond, G., Simatos, D., Catt, M., Dussap, C. G., & Gros, J. B. (1997). Modeling of the water-sucrose state diagram below 0 ^{o}C. *Carbohydrate Research*, *298*(3), 139–145.

Chirife, J. & Inglesias, H. (1978). Equations for fitting water sorption isotherms of foods. 1. Review. *Journal of Food Technology*, *13*(3), 159–174.

Cicerone, M. T. & Douglas, J. F. (2012). Beta-relaxation governs protein stability in sugar-glass matrices. *Soft Matter*, *8*, 2983–2991.

Cicerone, M. T., Pikal, M. J., & Qian, K. K. (2015). Stabilization of proteins in solid form. *Advanced Drug Delivery Reviews*, *93*, 14–24.

Couchman, P. R. & Karasz, F. E. (1978). A classical thermodynamic discussion of the effect of composition on glass transition temperatures. *Macromolecules*, *11*, 117–119.

Fox, T. G. (1956). Influence of diluent and copolymer composition on the glass transition of a polymer system. *Bulletin of the American Physical Society*, *1*, 123–132.

Frank, G. A. (2007). Measurement analysis of glass transition temperature for sucrose and trehalose aqueous solutions. *Journal of Physical and Chemical Reference Data*, *36*(4), 1279–1285.

Gordon, M. & Taylor, J. (1952). Ideal copolymers and the second order transitions of synthetic rubbers. *Journal of Applied Chemistry*, *2*, 493–500.

Greenspan, L. (1977). Humidity fixed points of binary saturated aqueous solutions. *Journal of Research of the National Bureau of Standards: A, Physics and Chemistry*, *81A*, 89–96.

Gunning, Y. M., Parker, R., & Ring, S. G. (2000). Diffusion of short chain alcohols from amorphous maltosewater mixtures above and below their glass transition temperature. *Carbohydrate Research*, *329*, 377–385.

Hansen, E. W., Kristiansen, P. E., & Pedersen, B. (1998). Crystallinity of polyethylene derived from solid-state proton NMR free induction decay. *The Journal of Physical Chemistry B*, *102*(28), 5444–5450.

Hourston, D., Song, M., Hammiche, A., Pollock, H., & Reading, M. (1997). Modulated differential scanning calorimetry: 6. Thermal characterization of multicomponent polymers and interfaces. *Polymer*, *38*(1), 1–7.

Hourston, D., Song, M., Schafer, F.-U., Pollock, H., & Hammiche, A. (1999). Modulated-temperature differential scanning calorimetry: 15. Crosslinking in polyurethane-poly(ethyl methacrylate) interpenetrating polymer networks. *Polymer*, *40*(17), 4769–4775.

Hughes, D., Tedeschi, C., Leuenberger, B., Roussenova, M., Coveney, A., Richardson, R., Bönisch, G. B., Alam, M. A., & Ubbink, J. (2016). Amorphous-amorphous phase separation in hydrophobically-modified starch-sucrose blends II. Crystallinity and local free volume investigation using wide-angle X-ray scattering and positron annihilation lifetime spectroscopy. *Food Hydrocolloids*, *58*, 316–323.

Kalichevsky, M., Jaroszkiewicz, E., Ablett, S., Blanshard, J., & Lillford, P. (1992). The glass transition of amylopectin measured by DSC, DMTA and NMR. *Carbohydrate Polymers*, *18*(2), 77–88.

Kalichevsky, M. T. & Blanshard, J. M. (1993). The effect of fructose and water on the glass transition of amylopectin. *Carbohydrate Polymers*, *20*(2), 107–113.

Kalichevsky, M. T., Jaroszkiewicz, E. M., & Blanshard, J. (1993). A study of the glass transition of amylopectinsugar mixtures. *Polymer*, *34*(2), 346–358.

Karel, M. (1990). Encapsulation and controlled release of food components. In H. G. Schwartzberg & M. A. Rao (Eds.), *Biotechnology and Food Process Engineering* (pp. 277–294). Marcel Dekker, Inc., New York.

Kasapis, S., Norton, I. T., & Ubbink, J. B. (Eds.). (2009). *Modern biopolymer science: bridging the divide between fundamental treatise and industrial application*. Elsevier.

Kilburn, D., Claude, J., Mezzenga, R., Dlubeck, G., Alam, A., & Ubbink, J. (2004). Water in glassy carbohydrates: Opening it up at the nanolevel. *Journal of Physical Chemistry B*, *108*, 12436–12441.

577 Kilburn, D., Claude, J., Schweizer, T., Alam, A., & Ubbink, J. (2005). Car-
578 bohydrate polymers in amorphous states: An integrated thermodynamic and
579 nanostructural investigation. *Biomacromolecules*, *6*, 864–879.

580 Kwei, T. (1984). The effect of hydrogen bonding on the glass transition tem-
581 perature of polymer mixtures. *Journal of Polymer Science*, *22*, 307–313.

582 Levine, H. (Ed.). (2002). *Amorphous Food and Pharmaceutical Systems*. Royal
583 Society of Chemistry.

584 Look, D. C., Lowe, I. J., & Northby, J. A. (1966). Nuclear magnetic resonance
585 study of molecular motions in solid hydrogen sulfide. *The Journal of Chemical*
586 *Physics*, *44*(9), 3441–3452.

587 Makower, B. & Dye, W. B. (1956). Sugar crystallization, equilibrium moisture
588 content and crystallization of amorphous sucrose and glucose. *Journal of*
589 *Agricultural and Food Chemistry*, *4*(1), 72–77.

590 Orford, P., Parker, R., Ring, S., & Smith, A. (1989). Effect of water as a
591 diluent on the glass transition behaviour of malto-oligosaccharides, amylose
592 and amylopectin. *International Journal of Biological Macromolecules*, *11*(2),
593 91–96.

594 Pake, G. E. (1948). Nuclear resonance absorption in hydrated crystals: Fine
595 structure of the proton line. *The Journal of Chemical Physics*, *16*(4), 327–336.

596 Reineccius, G. A. & Yan, C. (2016). Factors controlling the deterioration of
597 spray dried flavourings and unsaturated lipids. *Flavour and Fragrance Jour-*
598 *nal*, *31*(1), 5–21.

599 Roos, Y. H. (1995). *Phase Transitions in Foods*. Academic Press.

600 Roudaut, G., Farhat, I., Poirier-Brulez, F., & Champion, D. (2009). Influence of
601 water, temperature and sucrose on dynamics in glassy starch-based products
602 studied by low field ^{1}H NMR. *Carbohydrate Polymers*, *77*(3), 489–495.

603 Roudaut, G. & Wallecan, J. (2015). New insights on the thermal analysis of low
604 moisture composite foods. *Carbohydrate Polymers*, *115*, 10–15.

605 Roussenova, M. (2011). *Molecular organisation and mobility in glass forming
606 systems - a free volume perspective*. PhD thesis, University of Bristol.

607 Roussenova, M., Murith, M., Alam, A., & Ubbink, J. (2010). Plasticization,
608 antiplasticization, and molecular packing in amorphous carbohydrate-glycerol
609 matrices. *Biomacromolecules*, *11*, 3237–3247.

610 Saleki-Gerhardt, A. & Zografi, G. (1994). Non-isothermal and isothermal crys-
611 tallization of sucrose from the amorphous state. *Pharmaceutical Research*,
612 *11*(8), 1166–1173.

613 Schoonman, A., Ubbink, J., Bisperink, C., Meste, M. L., & Karel, M. (2002).
614 Solubility and diffusion of nitrogen in maltodextrin/protein tablets. *Biotech-
615 nology Progress*, *18*, 139–154.

616 Seow, C. C. (2010). Antiplasticization of food polymer systems by low molecular
617 mass diluents. In Reid, D. S., Sajjaanantakul, T., Lillford, P. J., & Charoen-
618 rein, S. (Eds.), *Water properties in food, health, pharmaceutical and biological
619 systems: ISOPOW 10*, (pp. 115–137).

620 Silaket, P., Chatakanonda, P., Tran, T., Wansuksri, R., Piyachomkwan, K.,
621 & Sriroth, K. (2014). Thermal properties of esterified cassava starches and
622 their maltodextrins in various water systems. *Starch - Starke*, *66*(11-12),
623 1022–1032.

624 Song, M., Hourston, D., Pollock, H., Schafer, F., & Hammiche, A. (1997).
625 Modulated differential scanning calorimetry: Xi. A characterisation method
626 for interpenetrating polymer networks. *Thermochimica Acta*, *304-305*, 335–
627 346. Temperature Modulated Calorimetry.

628 te Booy, M. P. W. M., de Ruiter, R. A., & de Meere, A. L. J. (1992). Evaluation
629 of the physical stability of freeze-dried sucrose-containing formulations by
630 differential scanning calorimetry. *Pharmaceutical Research*, *9*(1), 109–114.

631 Tedeschi, C., Leuenberger, B., & Ubbink, J. (2016). Amorphous-amorphous
632 phase separation in hydrophobically-modified starch-sucrose blends i. Phase
633 behavior and thermodynamic characterization. *Food Hydrocolloids*, *58*, 75–88.

634 Tizzotti, M. J., Sweedman, M. C., Tang, D., Schaefer, C., & Gilbert, R. G.
635 (2011). New ^{1}H NMR procedure for the characterization of native and modi-
636 fied food-grade starches. *Journal of Agricultural and Food Chemistry*, *59*(13),
637 6913–6919.

638 Townrow, S., Kilburn, D., Alam, M. A., , & Ubbink, J. (2007). Molecular pack-
639 ing in amorphous carbohydrate matrixes. *The Journal of Physical Chemistry*
640 *B*, *111*(44), 12643–12648.

641 Townrow, S., Roussenova, M., Giardello, M., Alam, A., & Ubbink, J. (2010).
642 Specific volume-hole volume correlations in amorphous carbohydrates: Effect
643 of temperature, molecular weight, and water content. *Journal of Physical*
644 *Chemistry B*, *114*, 1568–1578.

645 Tromp, R. H., Parker, R., & Ring, S. G. (1997). Water diffusion in glasses of
646 carbohydrates. *Carbohydrate Research*, *303*(2), 199–205.

647 Ubbink, J. (2016). Structural and thermodynamic aspects of plasticization and
648 antiplasticization in glassy encapsulation and biostabilization matrices. *Ad-*
649 *vanced Drug Delivery Reviews*, *100*, 10–26. Amorphous pharmaceutical solids.

650 Ubbink, J., Burbidge, A., & Mezzenga, R. (2008). Food structure and function-
651 ality: a soft matter perspective. *Soft Matter*, *4*, 1569–1581.

652 Ubbink, J., Giardiello, M.-I., & Limbach, H.-J. (2007). Sorption of water by
653 bidisperse mixtures of carbohydrates in glassy and rubbery states. *Biomacro-*
654 *molecules*, *8*(9), 2862–2873.

655 Ubbink, J. & Krüger, J. (2006). Physical approaches for the delivery of active
656 ingredients in foods. *Trends in Food Science & Technology*, *17*(5), 244–254.

Ubbink, J., Zwick, T., Hughes, D., & Bönisch, G. B. (2018). Water vapor sorption and glass transition temperatures of phase-separated amorphous blends of hydrophobically-modified starch and sucrose (in press). *Data In Brief*.

van der Sman, R. G. M. (2013). Predictions of glass transition temperature for hydrogen bonding biomaterials. *The Journal of Physical Chemistry B*, *117*, 16303–16313.

Graphical Abstract